On the Structure of Nonastannide Clusters in Liquid and Solid State

Jan Rosdahl,[a] Thomas F. Fässler,[b] and Lars Kloo*[a]

Keywords: EXAFS spectroscopy / Cluster compounds / Polyanions / Solid-state structures / Ab initio calculations

The nonastannide clusters have been investigated using EXAFS, NMR and Raman spectroscopy as well as quantum chemical calculations explicitly considering a model cationic field and solid-state statistics. NMR spectroscopic and EXAFS results are basically identical to those previously published and consistent with a fluctional model of the cluster. The quantum chemical calculations show that there is no significant difference in energy between the two model geometries, C_{4v} and D_{3h}, and that the vibrational frequencies are very low, clearly indicating that the cluster is expected to be fluctional. The solid-state statistics show that both model geometries can be used to describe all known nonastannide structures with reasonable success, illustrating that the classification of the nonastannide clusters in terms of specific symmetries is entirely arbitrary.

Introduction

Homoatomic clusters of the main-group elements, E_n, is a group of molecules that have attracted some interest over the last decades.[1–3] This is partly due to the fact that these clusters are considered to form one of many extensions to the exciting borane chemistry. However, when using heavier atoms the bonds become more flexible with regards to acceptable bond lengths and angles, as compared to the lighter elements. Good candidates for investigating such flexibility effects are the nine-vertex clusters with C_{4v} or D_{3h} symmetry, such as E_9^{4-} or E_9^{3-} (E = Ge, Sn or Pb), due to their highly related geometries. In order to simplify the matter somewhat, we will mainly focus on the nonastannide clusters.

Over the last three decades, several crystallographic structures containing Sn_9^{4-} or Sn_9^{3-} have been reported.[4–15] Several of these have been classified as having a C_{4v} geometry, as expected according to Wade's rules for a *nido* cluster such as Sn_9^{4-}.[16] However, some appear to adopt a D_{3h} geometry, which is typical for a *closo* geometry and expected for Sn_9^{2-}, but it is most certainly not the correct geometry for a *nido* cluster such as Sn_9^{4-}. The same has been observed for other elements and is not considered to be unusual, yet unexplained. Many of the structure determinations indicate that there is some "disorder" in the structure and sometimes the structure is described in terms of going from C_{4v} geometry towards D_{3h}, or vice versa. The description is, nevertheless, still very static and often neglects the information contained in the anisotropic displacement parameters (ADPs), which we will show is unfortunate.

The prediction of the dynamic behavior of Sn_9^{4-} is at least as old as one of the first structures and was later complemented by a NMR spectroscopic investigation in solution.[5,17] However, the energy barrier for the fluctional behavior of the cluster was never determined, despite the low temperatures used during the experiments. This fluctional behaviour can even be retained when incorporating $Pt_2(PPh_3)$ into the cluster,[18] while other additions are more questionable with regards to the fluctional behaviour.[19,20]

Many of the early theoretical results for nonastannide clusters are based on extended Hückel calculations and they all report that the C_{4v} geometry is more stable than D_{3h}.[21,22] This is in good agreement with both earlier and more recent results,[5,20] but the opposite result can also be obtained, indicating that the difference in energy is very small.[23]

Since the description of the behaviour of nonastannide clusters in solution and solid state is so inconsistent, we believe that one of them can not be entirely correct. In order to get a more coherent description of the nature of these clusters, we have conducted an investigation involving EXAFS, NMR and Raman spectroscopy as well as quantum chemical calculations explicitly considering the effect of the cationic field and solid-state statistics.

Results and Discussion

Spectroscopy

The NMR spectroscopic results for the nonastannide cluster in ethylenediamine (en) solution are essentially the

[a] Department of Chemistry, Inorganic Chemistry, Royal Institute of Technology,
10044 Stockholm, Sweden
[b] Lehrstuhl für Anorganische Chemie mit Schwerpunkt Neue Materialien, Technische Universität München,
Lichtenbergstr. 4, 85747 Garching, Germany

  DOI: 10.1002/ejic.200500043

same as those previous obtained, showing a heptet at a chemical shift of +1208 ppm and J = 264 Hz for the tin-potassium system in ethylenediamine, thus confirming the fluctional behaviour of the clusters in solution.[17,24] The integrated satellite peak intensities also confirm this interpretation, since the number of neighbours in the cluster is determined to be between four and five, as expected for a fluctional nine-atomic cluster that is close to both C_{4v} and D_{3h} symmetry.

The Raman spectroscopic results for the nonastannide cluster in en solution are also similar to previous results, displaying a peak at 155 cm^{-1} for the sample containing K and Sn with a ratio of 1:1.[25] This peak is assigned to the symmetrical breathing mode of vibration. Similar spectra were observed for the Na:Sn system. Furthermore, the position of the peak and the number of observed bands are not conclusive for either geometry.

EXAFS measurements have been conducted for three different samples corresponding to an en solution with Sn_9^{4-}, a solid with Sn_9^{4-} and a solid with Sn_9^{3-}. The expected result would be that all three samples should exhibit significantly different EXAFS patterns, since these three systems were chosen to represent three different classes, a fluctional cluster, a cluster with rigid C_{2v} geometry and a cluster with rigid D_{3h} geometry. However, all three samples give rise to very similar EXAFS traces, as can be seen in Figure 1 and Figure 2. The EXAFS pattern for the solution is somewhat more limited in resolution than those of the solids. Despite this, the similarities are hard to ignore. Furthermore, the EXAFS results for the two solids are almost identical to each other and thus consistent with a fluctional cluster model also in solid state (see Figure 1).

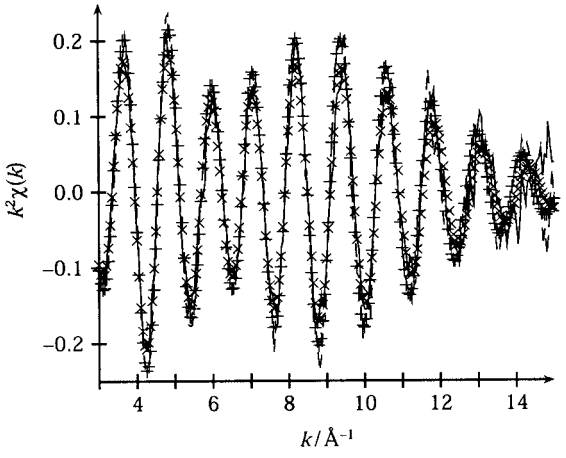

Figure 1. The reduced EXAFS data for the two solid model compounds. The solid line corresponds a solid with Sn_9^{3-}, while the dashed line corresponds to a solid with Sn_9^{4-}. The fitted models for the two samples are shown as × and +, respectively.

All three EXAFS traces can be fitted with a single Sn–Sn path, with a Sn–Sn distance of 3.06(4), 2.974(5)and 2.987(8) Å for the solution with Sn_9^{4-}, the solid with Sn_9^{4-} and the solid with Sn_9^{3-}, respectively. The problem with detecting longer distances is also consistent with a fluctional cluster model, since the largest variations are obtained for

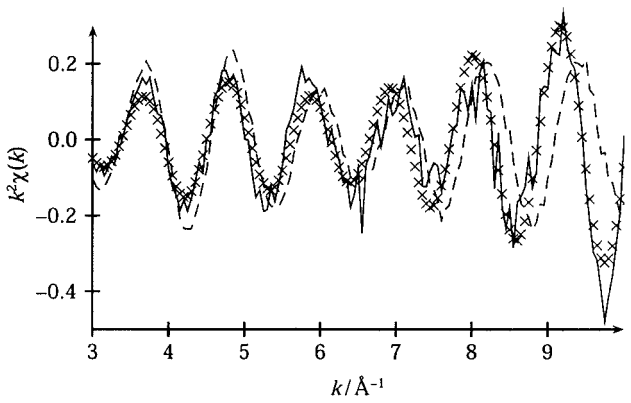

Figure 2. The reduced EXAFS data for the solution with Sn_9^{4-} (solid line) and fitted model (×). For comparison, the dashed line shows the solid with Sn_9^{4-}.

the longest Sn–Sn distances, thus dampening them below the level of noise. However, the longer Sn–Sn distances are present when calculating theoretical EXAFS spectra with rigid models of Sn_9^{4-}, both C_{4v} and D_{3h} geometries, and this is the only difference between experiment and theory (see Figure 3).

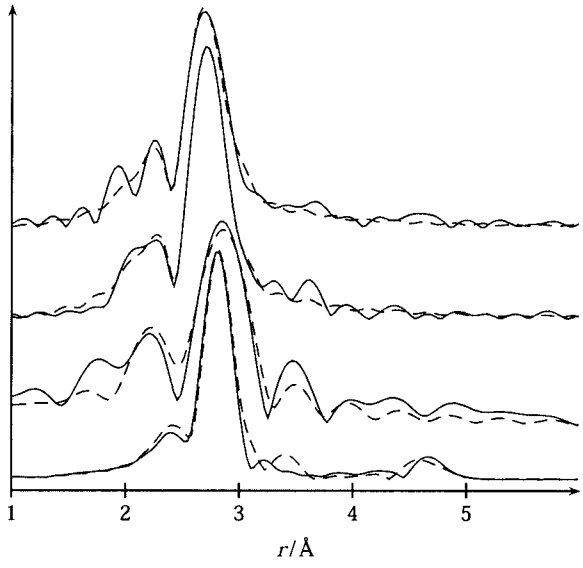

Figure 3. The radial distribution functions of the EXAFS data, fitted models and theoretical models. They are from top to bottom: solid sample with Sn_9^{3-} (solid line) and fitted model (dashed line); solid sample with Sn_9^{4-} (solid line) and fitted model (dashed line); solution with Sn_9^{4-} (solid line) and fitted model (dashed line); theoretical Sn_9^{4-} cluster with C_{4v} (solid line) and D_{3h} geometry (dashed line).

Solid-State Statistics

Several crystal structures of nonastannides are known, obtained at various temperatures and with different compositions.[4–15] The most common way to determine the symmetry of a cluster, when it is not very obvious, is to compare the angle and distance ratios with the idealised geometries.[26,9] A more blunt approach is to simply investigate the

histogram of intramolecular Sn–Sn distances, which exhibits some of the expected similarities with the EXAFS results, see Figure 3 and Figure 4. If the ratio between the number of distances that fall in the two regions $2.55 \leq d_{Sn-Sn} < 3.95$ and $3.95 \leq d_{Sn-Sn} \leq 5.15$, where d_{Sn-Sn} is the Sn–Sn distance in Å, is 7:5 (21:15) the cluster is classified as being more of D_{3h} type, while a ratio of 5:4 (20:16) is obtained for clusters being more of C_{4v} type. A naive explanation for the above ratios would be that a D_{3h} structure is expected to have 21 shorter distances; 12 between the capping atoms and the closest atoms in the prism, 6 within the triangles in the prism and 3 for the edges in the prism, and 15 longer distances. A similar reasoning for C_{4v} results in 20 shorter distances; 4 between the capping atom and the upper square, 4 within the lower square, 8 between the squares and 4 within the upper square, and 16 longer distances. However, both these approaches only consider the static positional information from the crystal structure determination and totally neglects the information in ADPs, which often constitute a large portion of the information of a crystallographic study.

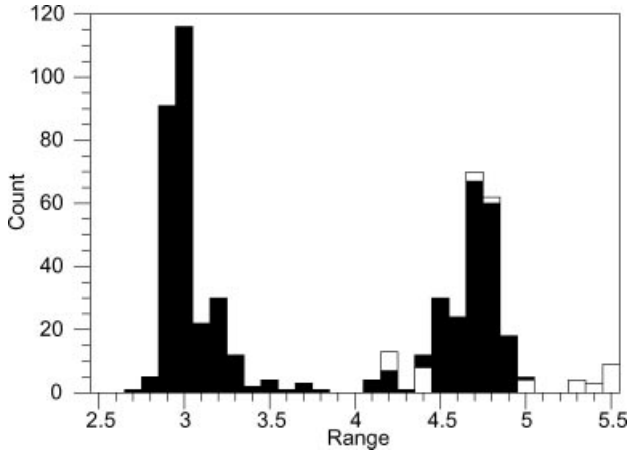

Figure 4. Histogram over intra (filled) and inter (open) molecular Sn–Sn distances.

We believe that the ADPs must be considered in order to get a more complete and dynamic picture of a solid-state structure. Therefore, we suggest that the symmetry of a cluster should be examined and possibly determined by fitting the idealised models to the crystallographic data, while considering the anisotropic displacement parameters. A nice feature with this approach is that the size of the ellipsoids needed to enclose the model using the experimental data will give an unbiased value of how good the fit is.

Since it is only necessary, more or less, to displace four of the nine atoms in order to change the symmetry from C_{4v} to D_{3h} or vice versa, it is evident that the remaining five atoms ought to fit both models reasonably well, which is clearly seen in Table 1, where the median of the fit never is worse than 30%. Moreover, ellipsoids with 80% probability is sufficient to include any of the two models in any of the structures, and ellipsoids with 50% probability will do the same for nearly half of the structures. This is also the level of the probability surfaces presented in most articles reporting solid-state structures.

The fit is generally better for the C_{4v} geometry compared to the D_{3h} one, mainly due to the extra parameter in the fit which is absent in the latter case. Furthermore, it can be seen that structures containing Sn_9^{3-} are better described in terms of a D_{3h} geometry than a C_{4v}, as expected, while structures containing Sn_9^{4-} often are better described in terms of a C_{4v} geometry. However, there are exceptions. Both models can be used, with reasonable success, to describe any of the nonastannide structures reported so far,

Table 1. Part of the statistical data for the various fits. The size of the ellipsoid needed to include the model is given in % and the distance between the experimental and the corresponding model position is given as d [Å].

	C_{4v}				D_{3h}				Combined						
	Max		Median		Max		Median		Max		Median				
System	%	d/Å	%	d/Å	%	d/Å	%	d/Å	%	d/Å	%	d/Å	Ratio	T/K	Ref.
$[K^+\text{-}([2,2,2]crypt)]_3[Sn_9]^{3-}(en)_{0.5}$	24.7	0.35	0.4	0.06	2.9	0.16	0.4	0.08	0.3	0.05	0.1	0.03	0.30	243	[10]
$[K^+\text{-}([2,2,2]crypt)]_3[Sn_9]^{3-}(en)_{1.5}$	60.2	0.46	3.3	0.12	0.2	0.04	0.1	0.02	0.2	0.04	0.1	0.02	0.01[a]	213	[6]
$[Na^+\text{-}([2,2,2]crypt)]_4[Sn_9]^{4-}$	0.4	0.07	0.1	0.03	39.9	0.38	10.3	0.20	0.3	0.06	0.1	0.03	0.96	278	[5]
$[K^+\text{-}([2,2,2]crypt)]_3[K^+][Sn_9]^{4-}$	0.4	0.06	0.2	0.04	51.2	0.38	24.8	0.23	0.2	0.04	0.1	0.03	0.92	173	[7]
$[K^+\text{-}([2,2,2]crypt)][Cs^+]_7([Sn_9]^{4-})_2(en)_3$	0.1	0.04	0.1	0.03	55.6	0.37	15.2	0.21	0.1	0.03	0.1	0.02	0.96	293	[12]
$[K^+\text{-}(18\text{-crown-}6)]_4[Sn_9]^{4-}(en)$	46.3	0.42	8.1	0.18	1.2	0.10	0.4	0.06	0.5	0.07	0.2	0.05	0.14[a]	193	[9]
$[K^+\text{-}(18\text{-crown-}6)]_3[K^+][Sn_9]^{4-}(en)$	17.5	0.27	3.6	0.14	5.2	0.16	1.6	0.12	0.5	0.06	0.1	0.04	0.36	243	[9]
$[Rb^+\text{-}(18\text{-crown-}6)]_2[Rb^+]_2[Sn_9]^{4-}(en)_{1.5}$	1.2	0.08	0.2	0.04	63.6	0.39	16.4	0.18	0.4	0.05	0.2	0.04	0.89	293	[13]
$[Na^+]_4[Sn_9]^{4-}(en)_7$	7.4	0.33	1.7	0.20	5.0	0.22	0.7	0.18	2.1	0.25	1.2	0.14	0.40[a]	293	[4]
$[Li^+\text{-}(NH_3)_4]_4[Sn_9]^{4-}(NH_3)$	0.4	0.04	0.1	0.02	80.2	0.37	25.1	0.17	0.2	0.02	0.1	0.01	0.93	123	[11]
$[K^+]_4[Sn_9]^{4-}$	3.1	0.10	0.4	0.06	51.8	0.35	17.6	0.19	1.5	0.08	0.4	0.05	0.87	293	[14]
$[Rb^+]_{12}[Sn_4]_2^{8-}[Sn_9]^{4-}$	5.7	0.15	1.5	0.08	58.8	0.42	28.7	0.23	5.3	0.15	2.0	0.08	0.95[b]	293	[15]
$[Rb^+]_{12}[Sn_4]_2^{8-}[Sn_9]^{4-}$	16.8	0.29	4.3	0.14	20.9	0.24	4.1	0.13	4.0	0.16	0.9	0.08	0.49[c]	293	[15]

[a] Better solutions exist for the combined model, $x\ C_{4v} + (1 - x)\ D_{3h}$, when x adopts a negative value. However, these were discarded since the fit was considered to be good enough even when x was limited to $0 \leq x \leq 1$. [b] This is for the structure where six of the atoms are labeled by an extra A and refined isotropically. [c] This is for the structure where six of the atoms are labeled by an extra B and refined.

clearly showing that the clusters are fluctional also in solid state and not only in solution (see Figure 5).

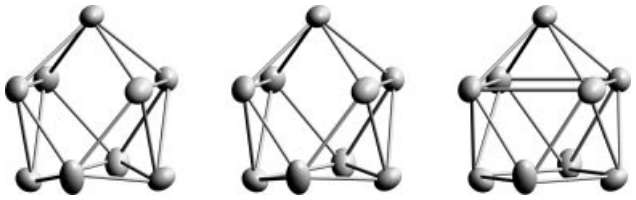

Figure 5. The three different models fitted to the same experimental data. They are from left to right; D_{3h}, C_{2v} and C_{4v}. The three-fold rotation axis in the case of D_{3h} is aligned horizontally. The crystallographic data being illustrated corresponds to $(K^+$-[18-crown-6]$)_3$-$[K^+][Sn_9]^{4-}$(en).[9]

An interesting feature of all the structures is that all tin atoms are located at general positions. This shows that all the clusters have unique geometries that are not directly enforced by the symmetry of the space group and that the different geometries most likely reflects the true nature of the clusters.

Theory

The calculational results clearly show that there is essentially no difference in energy between the two model symmetries, C_{4v} and D_{3h}, regardless the choice of basis set or theoretical method. The difference in energy between C_{4v} and D_{3h} being –3.5, –0.8 and +4.7 kJ·mol^{-1} at HF, B3LYP and MP2 levels, respectively, with the smallest basis set. The difference in energy is even smaller using larger basis sets, indicating that larger basis sets are required in order to properly describe the electron delocalisation in the cluster. Moreover, the preferred geometry appears to be dependent of the level of the calculation, illustrating the delicate balance between the different geometries in question. In addition, the vibrational frequencies are very low, highlighting that the potential energy surface is extremely flat for the two models (Table 2). Similar results have previously been reported, including the lead cluster congener.[20,27]

The obtained vibrational frequencies are lower than the experimentally observed ones, indicating that the harmonic oscillator approximation is not optimal.[25,20] Assuming that frequencies are reasonably correct, it immediately follows that the molecule will have several vibrational states occupied even at quite low temperatures. The most important vibrational mode is the lowest mode, the B_1 or E′, depending on the symmetry, whose vibrating motion is in the direction towards the alternative symmetry, see Figure 6. This shows that regardless of which of the two symmetries the cluster adopts it will always, as lowest vibrational mode, be vibrating in a manner that is directed towards the other symmetry. In this context it is noteworthy to remember that vibrational excitations correspond to larger oscillation amplitudes.

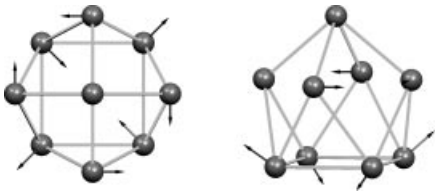

Figure 6. The displacement vectors for the lowest vibration mode of the theoretical model with C_{4v} geometry. In the left figure, the cluster is viewed upon along the C_4 axis, while in the right figure it is viewed almost perpendicularly to the C_4 axis.

The obtained vibrational frequencies are not particularly dependent on the choice of basis set, but the intensities are. This wouldn't be a problem if the relative intensities were

Table 2. Vibrational frequencies for the two model compounds at different levels of theory. Imaginary frequencies are shown as negative numbers and correspond to transition states (saddle points).

	HF		B3LYP		MP2	
Vibration	C_{4v}	D_{3h}	C_{4v}	D_{3h}	C_{4v}	D_{3h}
B_1:E'	26	–21	12	–7	–28	31
E:E′	51		44		51	
E:A_1'		82		74		78
B_1:E"	87	64	77	64	79	82
A_1:E"	82		81		89	
A_2:A_1"	70	95	71	87	93	98
B_2:E'	93	93	87	90	95	98
E:E'	90		85		98	
E:E"		94		90		101
B_2:E"	96		91		102	
E:A_2"	96	91	92	86	106	103
E:A_2'		96		91		109
A_1:E'	118	115	104	104	111	111
E:E'	125		113		120	
E:A_1'		128		115		120
B_1:E"	125	138	114	124	120	131
B_2:E"	140		127		135	
A_1:A_2"	139	141	130	129	140	137
E:A_1'	143	141	132	131	143	142
E:E'		147		134		146
A_1:E'	151		137		150	

left almost intact, but this is unfortunately not the case. However, a general trend is that the intensities increase with increasing number of diffuse functions in the basis set, which easily can be explained with the increased flexibility of the electron cloud.

The cationic field, introduced in an attempt to mimic more normal solid-state conditions for the cluster, leaves the vibrational frequencies almost unaffected, while having a significant impact on the total energy by mainly shifting the potential energies for the nuclei and electrons, resulting in a bound HOMO in a majority of the cases, see Figure 7 and Figure 8.

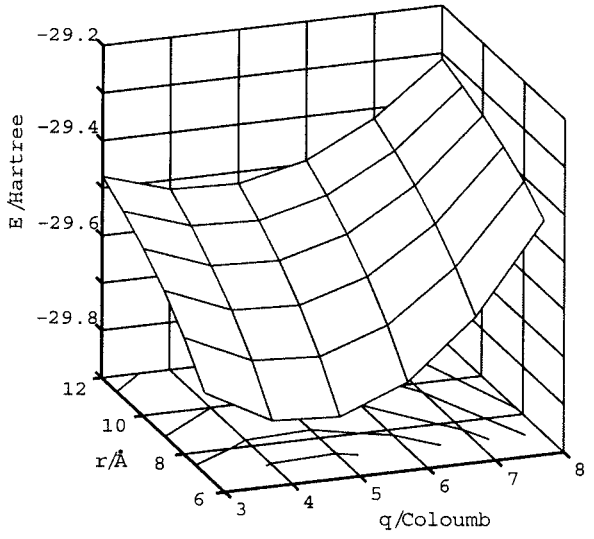

Figure 7. The variation of the total energy with respect to the radius and the charge of the cationic field for a Sn_9^{4-} cluster with C_{4v} geometry. The corresponding Figure for the D_{3h} geometry is virtually identical and thus not explicitly shown.

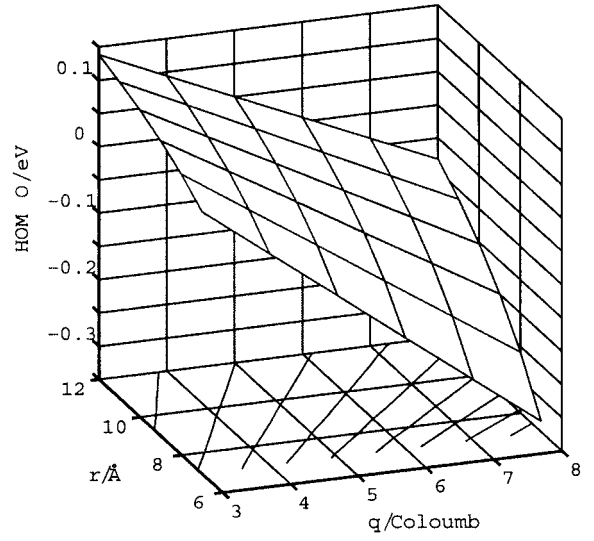

Figure 8. The variation of the HOMO energy level with respect to the radius and the charge of the cationic field for a Sn_9^{4-} cluster with C_{4v} geometry. The corresponding Figure for the D_{3h} geometry is virtually identical and thus not explicitly shown.

The ELF results are also practically unaffected by the field, and the differences are well within the expected accuracy of calculation.[28] Moreover, the iso-surfaces exhibit the same size, shape and location for the different cationic fields considered within the model geometries. This shows that the skeletal electrons are almost unaffected by the cationic field, thus leaving the polyhedral framework practically intact. When comparing iso-surfaces for the two model geometries, it becomes evident that they do not differ much at all, the largest difference in the enclosed iso-surface volumes is never larger than 2.2 Å^3 and this is less than 5% of the total volume in question (see Figure 9 and Figure 10).

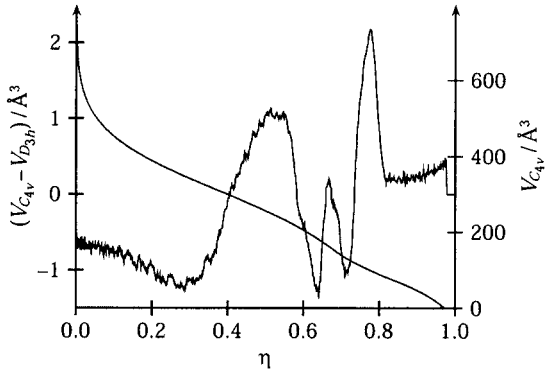

Figure 9. The difference in the enclosed iso-surface volumes between the C_{4v} and D_{3h} models together with the enclosed surface volume for the C_{4v} model at various η.

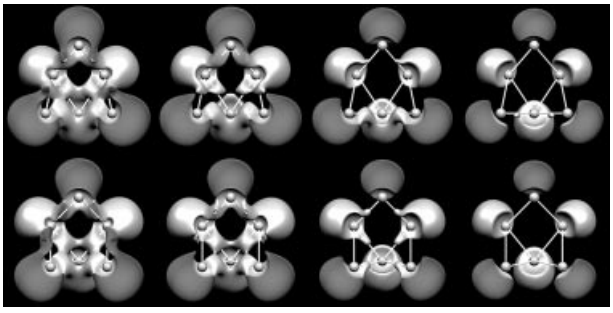

Figure 10. The iso-surfaces at η = 0.66, 0.69, 0.76 and 0.81, from left to right, for the optimised C_{4v} (upper) and D_{3h} geometry (lower). The surfaces are sliced through a σ_v mirror plane coinciding with the plane of the paper, i.e. the four-fold rotation axis for the C_{4v} model is aligned vertically in the plane of the paper and the three-fold rotation axis for the D_{3h} model is aligned horizontally in the plane of the paper.

Moreover, the preferred total charge for the field is about +5, slightly higher than the corresponding charge of the anionic cluster.

Conclusions

The nonstannide clusters are probably best viewed upon as highly fluctional, almost liquid-like drops that retain their fluctional behavior even in solid state and at low temperatures. Due to this fluctionality of the cluster it becomes superficial to discuss the symmetry of the cluster, since the only information known so far is the vibrational average and not the static ideal that is so vital for the discussion.

Experimental Section

Chemicals: Ethylenediamine (en, Merck, for synthesis, 99%) was refluxed with sodium for several hours, distilled under nitrogen and stored with molecular sieves before being used. Potassium metal (Alpha, 99.95%), sodium metal (Alpha, 99.95%) and tin metal (Baker, 99.98%) was used as purchased. The two solid samples, $(K^+$-[2,2,2]crypt$)_3[Sn_9]^{3-}$ and $(K^+$-[18-crown-6]$)_3[K^+][Sn_9]^{4-}$(en), were prepared as described elsewhere.[10,9]

Syntheses: The alloys were made by fusing the elements in a dry pyrex tube at 250 °C and with the molar ratios 10:1, 5:1, 1:1, 1:5 and 1:10 between potassium or sodium and tin. Ethylenediamine was added to the tube after the reaction was completed and the reaction mixture was allowed to equilibrate for 24 hours before further analysis of the solution. All work was carried out in a glove box with a dry nitrogen atmospehere (< 1 ppm O_2, < 1 ppm H_2O) due to the alloys sensitivety to oxygen.

NMR Spectroscopy: NMR spectra were recorded with a Varian Unity 300 MHz spectrometer operating at 111.87 MHz for ^{119}Sn. Chemical shifts are given with respect to $SnCl_4$ at +150 ppm.

Raman Spectroscopy: Raman spectra were obtained with a Bio-Rad Fourier Transform Raman system, employing the 1024 nm radiation of an infrared Nd:YAG laser. 4 cm^{-1} resolution was used.

EXAFS: X-ray absorption (EXAFS) data were recorded at the Stanford Synchrotron Radiation Laboratory (SSRL), using beam line 4 at 3.0 GeV and 50–90 mA. Monochromatic radiation was obtained from a Si(220) double crystal monochromator. High-order harmonics were rejected by 50% detuning. Incident and transmitted X-rays were monitored with argon-filled ion chambers. Six scans were made for all samples. The solid samples were contained in a cell of 1 mm thickness with Kapton film as windows, internally referenced by the K-edge of a tin foil to 29.2 keV. The liquid sample was contained in a cell of 2 mm thickness with Kapton film as windows and the fluorescence was detected with a Ge-detector after passing through an Ag filter. The FEFF program was employed to calculate the Sn–Sn phase shift and amplitude functions, which were used in the non-linear, least-squares fit of the k^3-weighted EXAFS data.[29,30]

Solid-State Statistics: The models were fitted to the crystallographic data with an in-house developed program, using the least-squares method minimising:

$$\sum_i \Delta X_i^T U_i^{-1} \Delta X_i$$

where ΔX_i is the positional difference between the model and the crystallographic data and U_i is the anisotropic displacement parameter for the i:th atom. Three different models were considered, C_{4v}, D_{3h} and a mixture of the two, $x\ C_{4v} + (1 - x)\ D_{3h}$. The last model was mainly used for determining the ratio between the two other ones, when the two models are oriented in such way that the combined model will have C_{2v} symmetry. Both models were fitted simultaneously to the data in order to limit the possibility of obtaining unrealistic results.

Common for all models is that there are three parameters related to the orientation of the model relative to the data. In addition, there are four and three parameters related to the size and shape of the C_{4v} and D_{3h} models, respectively. The combined model has an additional parameter related to the mixing of the two previous models. Thus, in total there are 7, 6 and 11 parameters that are fitted for the C_{4v}, D_{3h} and $x\ C_{4v} + (1 - x)\ D_{3h}$ models, respectively.

Calculations: All quantum chemical calculations, except the Electron Localisation Functions (ELF), were performed using Gaussian98 (rev. A7) with a variety of computers.[31] ECP-based basis sets were used for tin, employing the Stuttgart group, quasi-relativistic ECP's (46 and 28 core electrons) and slightly modified valence spaces;[32] (14s10p2d1f)/[3s3p2d1f] and (14s10p3d2f)/[4s4p3d2f] for the 46 core electron ECP, and (12s12p8d2f1g)/[6s6p3d2f1g] for the 28 core electron ECP.[33,34] Calculations were performed at Hartree–Fock (HF), B3LYP and 2nd-order Møller–Plesset perturbation theory (MP2) level and vibrational frequency calculations were performed.

The ELF calculations were performed using the TopMod program package.[28,35] The grid was chosen so that the distance between the borders and the closest atom was at least 6.0 a.u., and the step size was never larger than 0.1 a.u. The ELF iso-surfaces were visualised with the program Molekel.[36,37]

The cationic field was entered as point charges located at the vertices of a truncated icosahedron, more known as a buckyball or a football. The radius was varied between 7.0 and 12.0 Å at 1.0 Å interval and the point charges were uniformly assigned so that the total charge was varied between 3.0 and 8.0 Coulomb at 1.0 Coulomb interval. The center of the truncated icosahedron was aligned with the center of the molecule and a five-fold rotation axis was aligned with the rotational axis of the highest order of the molecule and another five-fold rotation axis was aligned with a suitable mirror plane, thus assuring that both symmetries are broken by the cationic field.

Acknowledgments

We are grateful to The Swedish Research Council and EU RTN for supporting this work. The authors thank Per Persson, Umeå University, for helpful discussions. Portions of this research were carried out at the Stanford Synchrotron Radiation Laboratory, a national user facility operated by Stanford University on behalf of the U.S. Department of Energy, Office of Basic Energy Sciences.

[1] J. D. Corbett, *Chem. Rev.* **1985**, *85*, 383–397.
[2] J. D. Corbett, *Angew. Chem. Int. Ed.* **2000**, *39*, 670–690.
[3] T. F. Fässler, *Coord. Chem. Rev.* **2001**, *215*, 347–377.
[4] L. Diehl, K. Khodadadeh, D. Kummer, J. Strähle, *Chem. Ber.* **1976**, *109*, 3404–3418.
[5] J. D. Corbett, P. A. Edwards, *J. Am. Chem. Soc.* **1977**, *99*, 3313–3317.
[6] S. C. Critchlow, J. D. Corbett, *J. Am. Chem. Soc.* **1983**, *105*, 5715–5716.
[7] R. C. Burns, J. D. Corbett, *Inorg. Chem.* **1985**, *24*, 1489–1492.
[8] T. F. Fässler, M. Hunziker, *Z. Anorg. Allg. Chem.* **1996**, *622*, 837–844.
[9] T. F. Fässler, R. Hoffmann, *Angew. Chem. Int. Ed. Angew. Chem. Int. Ed. Engl.* **1999**, *38*, 543–546.
[10] T. F. Fässler, R. Hoffmann, *Z. Kristallogr.-New Crystal Structures* **2000**, *215*, 139–142.
[11] N. Korber, A. Fleischmann, *J. Chem. Soc., Dalton Trans.* **2001**, 383–385.
[12] R. Hauptmann, R. Hoffmann, T. F. Fässler, *Z. Anorg. Allg. Chem.* **2001**, *627*, 2220–2224.
[13] R. Hauptmann, T. F. Fässler, *Z. Anorg. Allg. Chem.* **2002**, *628*, 1500–1504.
[14] C. Hoch, M. Wendorff, C. Röhr, *Acta Crystallogr., Sect. C* **2002**, *58*, 45–46.
[15] C. Hoch, M. Wendorff, C. Röhr, *J. Alloys Compd.* **2003**, *361*, 206–221.
[16] K. Wade, *Adv. Inorg. Chem. Radiochem.* **1976**, *18*, 1–66.

[17] R. W. Rudolph, W. L. Wilson, F. Parker, R. C. Taylor, D. C. Young, *J. Am. Chem. Soc.* **1978**, *100*, 4629–4630.
[18] B. Kesanli, J. Fettinger, D. R. Gardner, B. Eichhorn, *J. Am. Chem. Soc.* **2002**, *124*, 4779–4786.
[19] B. Kesanli, J. Fettinger, B. Eichhorn, *Chem. Eur. J.* **2001**, *7*, 5277–5285.
[20] J. Campbell, H. P. A. Mercier, H. Franke, D. P. Santry, D. A. Dixon, G. J. Schrobilgen, *Inorg. Chem.* **2002**, *41*, 86–107.
[21] L. L. Lohr Jr., *Inorg. Chem.* **1981**, *20*, 4229–4235.
[22] R. C. Burns, R. J. Gillespie, J. A. Barnes, M. J. McGlinchey, *Inorg. Chem.* **1982**, *21*, 799–807.
[23] A. Hirsch, Z. Chen, H. Jao, *Angew. Chem. Int. Ed.* **2001**, *40*, 2834–2838.
[24] W. L. Wilson, *Preparation and NMR Characterization of tin and lead Anionc Clusters*, Ph. D. thesis, The University of Michigan, **1982**.
[25] H. G. von Schnering, M. Baitinger, U. Bolle, W. Carrillo-Cabrera, J. Curda, Y. Grin, F. Heinemann, J. Llanos, K. Peters, A. Schmeding, M. Somer, *Z. Anorg. Allg. Chem.* **1997**, *623*, 1037–1039.
[26] L. J. Guggenberger, E. L. Muetterties, *J. Am. Chem. Soc.* **1976**, *98*, 7221–7225.
[27] J. Campbell, D. A. Dixon, H. P. A. Mercier, G. J. Schrobilgen, *Inorg. Chem.* **1995**, *34*, 5798–5809.
[28] S. Noury, X. Krokidis, F. Fuster, B. Silvi, *Computers & Chemistry* **1999**, *23*, 597–604.
[29] A. L. Ankudinov, B. Ravel, J. J. Rehr, S. D. Conradson, *Phys. Rev. B.* **1998**, *58*, 7565–7576.
[30] M. Newville, *J. Synchrotron Radiat.* **2001**, *8*, 322–324.
[31] M. J. Frisch, G. W. Trucks, H. B. Schlegel, G. E. Scuseria, M. A. Robb, J. R. Cheeseman, V. G. Zakrzewski, J. A. Montgomery, Jr., R. E. Stratmann, J. C. Burant, S. Dapprich, J. M. Millam, A. D. Daniels, K. N. Kudin, M. C. Strain, O. Farkas, J. Tomasi, V. Barone, M. Cossi, R. Cammi, B. Mennucci, C. Pomelli, C. Adamo, S. Clifford, J. Ochterski, G. A. Petersson, P. Y. Ayala, Q. Cui, K. Morokuma, D. K. Malick, A. D. Rabuck, K. Raghavachari, J. B. Foresman, J. Cioslowski, J. V. Ortiz, A. G. Baboul, B. B. Stefanov, G. Liu, A. Liashenko, P. Piskorz, I. Komaromi, R. Gomperts, R. L. Martin, D. J. Fox, T. Keith, M. A. Al-Laham, C. Y. Peng, A. Nanayakkara, C. Gonzalez, M. Challacombe, P. M. W. Gill, B. Johnson, W. Chen, M. W. Wong, J. L. Andres, C. Gonzalez, M. Head-Gordon, E. S. Replogle, J. A. Pople, *Gaussian 98, Revision A.7*. Gaussian, Inc., Pittsburgh PA, **1998**.
[32] The most diffuse functions were removed from the contracted part of the basis set.
[33] A. Bergner, M. Dolg, W. Kuechle, H. Stoll, H. Preuss, *Mol. Phys.* **1993**, *80*, 1431–1441.
[34] J. M. L. Martin, A. Sundermann, *J. Chem. Phys.* **2001**, *114*, 3408–3420.
[35] S. Noury, X. Krokidis, F. Fuster, B. Silvi, *TopMod package*, **1997**.
[36] P. Flükiger, H. P. Lüthi, S. Portmann, J. Weber, *MOLEKEL 4.3*, **2000–2002**.
[37] S. Portmann, H. P. Lüthi, *Chimia* **2000**, *54*, 766–770.

Received: January 13, 2005
Published Online: June 17, 2005

